Rainfall estimation by inverting SMOS soil moisture estimates: A comparison of different methods over Australia

Luca Brocca, Thierry Pellarin, Wade T. Crow, Luca Ciabatta, Christian Massari, Dongryeol Ryu, Chun-Hsu Su, Christoph Rüdiger, Yann Kerr

AGU PUBLICATIONS

JGR

Journal of Geophysical Research: Atmospheres

RESEARCH ARTICLE
10.1002/2016JD025382

Key Points:
- Comparison of three methods for estimating and correcting rainfall by using SMOS soil moisture data in Australia
- SMOS soil moisture data are able to improve the accuracy of "top down" satellite rainfall product available in real time (3B42RT)
- The integration of "bottom up" and "top down" approaches has high potential for delivering high-quality satellite rainfall products

Supporting Information:
- Supporting Information S1

Correspondence to:
L. Brocca,
luca.brocca@irpi.cnr.it

Citation:
Brocca, L., T. Pellarin, W. T. Crow, L. Ciabatta, C. Massari, D. Ryu, C.-H. Su, C. Rüdiger, and Y. Kerr (2016), Rainfall estimation by inverting SMOS soil moisture estimates: A comparison of different methods over Australia, *J. Geophys. Res. Atmos.*, *121*, 12,062–12,079, doi:10.1002/2016JD025382.

Received 18 MAY 2016
Accepted 6 OCT 2016
Accepted article online 8 OCT 2016
Published online 25 OCT 2016

Rainfall estimation by inverting SMOS soil moisture estimates: A comparison of different methods over Australia

Luca Brocca[1], Thierry Pellarin[2], Wade T. Crow[3], Luca Ciabatta[1], Christian Massari[1], Dongryeol Ryu[4], Chun-Hsu Su[4], Christoph Rüdiger[5], and Yann Kerr[6]

[1]Research Institute for Geo-hydrological Protection, National Research Council, Perugia, Italy, [2]LTHE, University Grenoble Alpes, CNRS, Grenoble, France, [3]Hydrology and Remote Sensing Laboratory, USDA-ARS, Beltsville, Maryland, USA, [4]Department of Infrastructure Engineering, University of Melbourne, Melbourne, Victoria, Australia, [5]Department of Civil Engineering, Monash University, Clayton, Victoria, Australia, [6]Centre d'Etudes Spatiales de la Biosphère, CNES CNRS IRD UPS, Toulouse, France

Abstract Remote sensing of soil moisture has reached a level of maturity and accuracy for which the retrieved products can be used to improve hydrological and meteorological applications. In this study, the soil moisture product from the Soil Moisture and Ocean Salinity (SMOS) satellite is used for improving satellite rainfall estimates obtained from the Tropical Rainfall Measuring Mission multisatellite precipitation analysis product (TMPA) using three different "bottom up" techniques: SM2RAIN, Soil Moisture Analysis Rainfall Tool, and Antecedent Precipitation Index Modification. The implementation of these techniques aims at improving the well-known "top down" rainfall estimate derived from TMPA products (version 7) available in near real time. Ground observations provided by the Australian Water Availability Project are considered as a separate validation data set. The three algorithms are calibrated against the gauge-corrected TMPA reanalysis product, 3B42, and used for adjusting the TMPA real-time product, 3B42RT, using SMOS soil moisture data. The study area covers the entire Australian continent, and the analysis period ranges from January 2010 to November 2013. Results show that all the SMOS-based rainfall products improve the performance of 3B42RT, even at daily time scale (differently from previous investigations). The major improvements are obtained in terms of estimation of accumulated rainfall with a reduction of the root-mean-square error of more than 25%. Also, in terms of temporal dynamic (correlation) and rainfall detection (categorical scores) the SMOS-based products provide slightly better results with respect to 3B42RT, even though the relative performance between the methods is not always the same. The strengths and weaknesses of each algorithm and the spatial variability of their performances are identified in order to indicate the ways forward for this promising research activity. Results show that the integration of bottom up and top down approaches has the potential to improve the quality of near-real-time rainfall estimates from remote sensing in the near future.

1. Introduction

Precipitation is one of the key components in the hydrologic cycle, and, consequently, its assessment is essential for many applications in geosciences. Precipitation data are essential to weather forecasting, food security, agricultural modeling, and emergency response planning [*McBride and Ebert*, 2000; *Hou et al*., 2014]. While long-term precipitation patterns are needed for climate studies and for drought monitoring [*van Dijk et al*., 2013; *Herold et al*., 2015; *Sahoo et al*., 2015], near-real-time precipitation data are critical for better understanding the spread of vector-borne and waterborne diseases [*Hunter*, 2003; *Scholthof*, 2006; *Rinaldo et al*., 2012] and for the mitigation of the impacts of natural disasters such as floods and landslides [*Guzzetti et al*., 2007; *Wake*, 2013; *Wu et al*., 2014].

Rain gauges provide the most common and most direct measurement of point precipitation at the surface; therefore, they are generally assumed as the most accurate method to measure precipitation [*Lanza and Vuerich*, 2009]. However, despite their relative accuracy, the distribution of available gauges varies significantly around the world [*Kucera et al*., 2013; *Schamm et al*., 2013]. For instance, *New et al*. [2001] estimate the number of gauges worldwide to be about 250,000 which is a relatively small number comparing to the extension of the landmass. The physical characteristics of precipitation, particularly at finer spatial and temporal resolutions, necessitate frequent and systematic measurements. The current networks of surface observations are

therefore often inadequate for the quantitative assessment of precipitation over large areas. The use of weather radar addresses some of the issues of rain gauge coverage, at least where radar exists. In particular, it provides a spatial measurement of precipitation rather than the point measurement provided by gauges. However, weather radars suffer from several issues due to the calibration of the empirical relation between reflectivity and rainfall rate, atmospheric attenuation, frozen hydrometeors, beam blockage, and range effects [e.g., *Krajewski and Smith*, 2002; *Delrieu et al*., 2009].

Satellite-based remote sensing of precipitation has advanced significantly over the last decade [*Kidd and Levizzani*, 2011] starting with the success of the Tropical Rainfall Measuring Mission multisatellite precipitation analysis products (TMPA) [*Huffman et al*., 2007] through to the deployment of the Global Precipitation Measurement (GPM) Mission satellite constellation (http://pmm.nasa.gov/GPM) [*Hou et al*., 2014]. Under the GPM mission, a constellation of satellite sensors is currently employed for estimating rainfall from space, with broad coverage of Earth at any given time of day. The retrieval of rainfall in the state-of-the-art satellite products is based on a "top down" approach; i.e., rainfall is obtained through the inversion of the atmospheric signals scattered or emitted by hydrometeors [*Kucera et al*., 2013]. At the overpass time of microwave sensors (radiometers and radars), the instantaneous rainfall rate is estimated and then (in some rainfall products) blended between successive overpasses by using infrared measurements from geostationary satellites [*Kidd and Levizzani*, 2011]. Top down rainfall products have the important advantage of being able to estimate different types of precipitation (including snowfall, drizzle, and hail) and are based on >25 year heritage of research. However, because of its inherently intermittent nature (i.e., high temporal variability), it is difficult to reliably determine rainfall with a limited amount of instantaneous observations [*Hossain and Anagnostou*, 2004; *Serrat-Capdevila et al*., 2014; *Trenberth*, 2014], which is particularly challenging for convective precipitation events. Other important limitations of those state-of-the-art products are related to (1) the estimation of low rainfall intensities, especially over land due to the confounding effects of surface emissivity [*Tapiador et al*., 2012; *Pipunic et al*., 2015]; (2) the large bias of the real-time products detected in many parts of the world [*Kucera et al*., 2013]; (3) the difficulties in estimating rainfall in semiarid climates and for low-intensity stratiform precipitation [*Ebert et al*., 2007]; and (4) the assessment of solid precipitation in cold climates (e.g., Arctic regions) [*Hou et al*., 2014].

For hydrologic applications, the continuity of data over an accumulation window suitable for a particular goal is more important than having highly accurate estimates of instantaneous rain rates [*Ciabatta et al*., 2016]. These accumulation periods can range between ~15 min for flash flood forecasting to weekly for agricultural applications and monthly for climate analysis. For instance, even a small underestimation or overestimation of rainfall in some days (e.g., due to undersampling) produces errors in the simulation of the system state in rainfall-runoff applications (i.e., the soil moisture storage), and, consequently, it induces larger errors in the estimation of runoff due to the strong nonlinearity between soil moisture and runoff [*Koster et al*., 2010; *Brocca et al*., 2012]. In other words, the memory of the hydrological systems magnifies the error in the accumulated rainfall over time. Similar issues can be recognized in the prediction of landslide occurrence or in agricultural applications. Therefore, there is a clear need to maximize the accuracy of satellite products in the estimation of accumulated rainfall [*Serrat-Capdevila et al*., 2014; *Maggioni et al*., 2016].

In order to better quantify precipitation, a "bottom up" approach was recently proposed for correcting and/or estimating rainfall over land by the exploitation of satellite soil moisture data [*Crow et al*., 2009, 2011; *Pellarin et al*., 2008, 2013; *Brocca et al*., 2013, 2014; *Ciabatta et al*., 2015; *Wanders et al*., 2015; *Zhan et al*., 2015]. The underlying assumption is very simple. After a rainfall pulse, soil moisture exhibits a sudden increase followed by a smooth recession limb driven by evapotranspiration and drainage. An increase of soil moisture can thus be related to the accumulated rainfall suggesting the use of soil moisture for rainfall estimation [e.g., *Brocca et al*., 2013] or correction [e.g., *Crow et al*., 2009]. A first approach consists on using exclusively soil moisture data as an indirect signature of the rainfall dynamic and to reconstruct the precipitation time series. Recent work by *Brocca et al*. [2013, 2014] investigates this approach in the so-called SM2RAIN algorithm that, by inverting the soil water balance equation, allows to estimate rainfall directly from soil moisture observations. A second kind of approach makes use of a Land Surface Model (LSM) forced with a satellite-based precipitation product to exploit the potential differences between simulated (by LSM) and satellite-retrieved surface soil moisture [*Pellarin et al*., 2008; *Crow et al*., 2009, 2011; *Pellarin et al*., 2013; *Wanders et al*., 2015]. These differences are analyzed for correcting the satellite-based precipitation product. Specific examples of such methods include the Soil Moisture Analysis Rainfall Tool (SMART) [*Crow et al*., 2011] and the Antecedent Precipitation Index Modification (API-mod) [*Pellarin et al*., 2013] approaches.

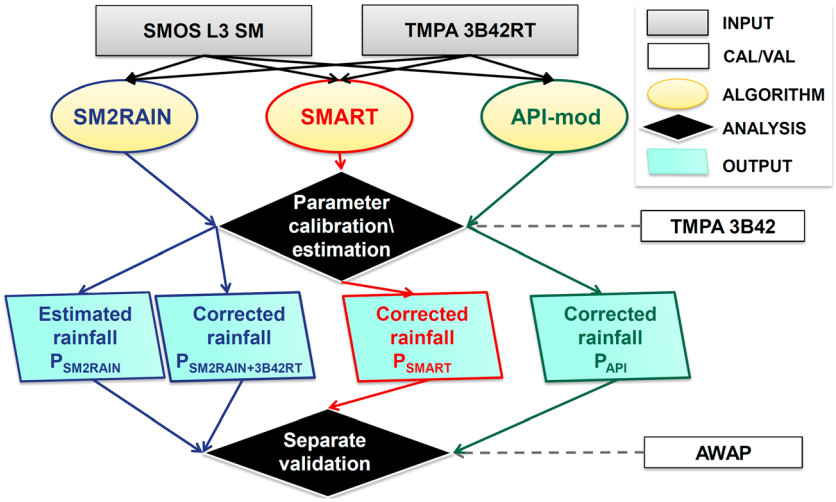

Figure 1. Diagram of the input-output data, algorithms, and processing step carried out in the study for estimating and correcting rainfall through SMOS soil moisture observations. Note that TMPA 3B42 and AWAP data sets are used for parameter calibration/estimation and products validation, respectively.

The main purpose of this study is to investigate the potential of correcting real-time satellite rainfall products using satellite soil moisture observations. To achieve this, three different algorithms are applied for integrating remotely sensed soil moisture and rainfall data over the Australian main continent: SM2RAIN [*Brocca et al*., 2014], API-mod [*Pellarin et al*., 2013], and SMART [*Crow et al*., 2011]. This represents the first formal comparison of these three independently developed approaches. The required satellite soil moisture observations are obtained from the European Space Agency led Soil Moisture and Ocean Salinity (SMOS) mission version 5.51 (RE02) data set, provided by the Centre Aval de Traitement des Données SMOS (CATDS, Level 3 product). 3B42RT and 3B42, the real-time and gauge-corrected TMPA products (version 7), respectively, are used as the top down satellite rainfall products. Specifically, the TMPA 3B42 reanalysis product is used as reference for the calibration of the parameter values of the three algorithms, in the course of correcting errors in the 3B42RT product using satellite soil moisture observations. To evaluate the performance of the rainfall products and their algorithms, the gauge-based rainfall data set from the Australian Water Availability Project (AWAP) is employed. The gridded AWAP product is produced by spatial interpolation of daily rain gauge measurements across the continent [*Jones et al*., 2009]. For the analysis, all the data sets are resampled at 0.25° spatial resolution and daily time step for the period 15 January 2010 to 30 November 2013.

2. Methods

As mentioned above, the main purpose of the study is to perform a detailed analysis of three different methods that can be used for improving satellite rainfall estimation using remotely sensed soil moisture data, namely, SM2RAIN [*Brocca et al*., 2014], API-mod [*Pellarin et al*., 2013], and SMART [*Crow et al*., 2011]. The main benefit of this study is that the three different methods are applied by using the same input data and the same analysis period thus allowing to perform a fair, comprehensive, and robust comparison. The Australian continent is selected as case study because of satellite soil moisture observations from SMOS that are known to be accurate [e.g., *Al-Yaari et al*., 2014a, 2014b] and also for the availability of the good quality gauge-based AWAP product which allows for an objective evaluation of the three algorithms. The real-time version of TMPA (3B42RT) is used as input along with SMOS soil moisture observations (ascending plus descending orbits). We underline that the analysis was carried out also by considering ascending and descending SMOS orbits separately (results are not shown); however, the best results are obtained by using both overpasses. The gauge-corrected TMPA product, 3B42, is used for a pixel-by-pixel calibration of the parameter values of the three algorithms. The gauge-based AWAP product is finally employed as a separate validation data set (see the diagram in Figure 1). We acknowledge that AWAP and 3B42 data sets are not fully independent as the gauge correction of 3B42 product likely includes some of the AWAP gauges. However, as

the correction is made at monthly time scale, it is less important at 1 day and 5 day time scales that are considered here for evaluating the candidate algorithms. Due to limitations in the current length of the SMOS soil moisture data set, distinct temporal periods for parameter calibration and model validation are not utilized.

Each product is resampled in space to the same computational grid with spacing of 0.25° Equal-Area Scalable Earth (EASE) (EASE grid). The temporal resolution of the obtained rainfall products is daily (9 A.M. to 9 A.M., local standard time, as AWAP). Both the parameter calibration and the performance assessment are carried out for the whole data period, i.e., from 15 January 2010 to 30 November 2013.

In the following sections, the main characteristics of each algorithm, and their specific implementation for this study, are summarized. More complete descriptions of each method can be obtained in the cited references.

2.1. SM2RAIN

SM2RAIN [*Brocca et al*., 2014] is a simple algorithm for estimating rainfall accumulations through the knowledge of soil moisture observations. To calculate the rainfall at a given time step, the method inverts a single-layer soil water balance model using soil moisture observations at current and previous time steps and assumes that during a rainfall event evapotranspiration and surface runoff contributions are negligible. Previous global applications of the model under varying precipitation regimes [*Brocca et al*., 2014, 2015] have provided evidence for the validity of those assumptions. That is,

$$P_{\mathrm{SM2RAIN}}(t) = Z^{*}\mathrm{d}s(t)/\mathrm{d}t + as(t)^{b} \tag{1}$$

where P_{SM2RAIN} [L/T] is the estimated rainfall, s [$-$] is the relative saturation of the soil (between 0 and 1), t [T] is the time, Z^{*} [L] is the soil water capacity (soil layer depth multiplied by porosity), and a [L/T] and b [$-$] are two parameters expressing the nonlinearity between the loss rate (including both the drainage and the evapotranspiration components) and soil saturation. In equation (1), negative rainfall values, which occur during some dry-down cycles, are set equal to zero.

Since satellite soil moisture observations are affected by potentially considerable high-frequency variations (noise), the exponential filter first proposed by *Wagner et al*. [1999] is used for noise reduction [*Su et al*., 2013]. In this respect, the calibration of the only parameter of the filter T (characteristic time length) is performed together with SM2RAIN parameters Z^{*}, a, and b.

For merging the SM2RAIN-derived rainfall estimates with the real-time satellite rainfall product (3B42RT), P_{3B42RT}, a simple nudging scheme is adopted [*Ciabatta et al*., 2015; *Massari et al*., 2014]:

$$P_{\mathrm{SM2RAIN+3B42RT}}(t) = P_{\mathrm{3B42RT}}(t) + k[P_{\mathrm{SM2RAIN}}(t) - P_{\mathrm{3B42RT}}(t)] \tag{2}$$

where $P_{\mathrm{SM2RAIN+3B42RT}}$ [L/T] is the rainfall merged product of SM2RAIN and 3B42RT and k [$-$] has the same role of the Kalman gain in Kalman filtering techniques with the difference that in this case, it determines the relative weight of the uncertainty in P_{3B42RT} against the one of the SM2RAIN prediction, P_{SM2RAIN}.

The SM2RAIN algorithm provides two rainfall products (Figure 1), i.e., P_{SM2RAIN} and $P_{\mathrm{SM2RAIN+3B42RT}}$, and involves four ($Z^{*}$, a, b, and T) and five (Z^{*}, a, b, T, and k) parameters to be calibrated for P_{SM2RAIN} and $P_{\mathrm{SM2RAIN+3B42RT}}$, respectively, on a pixel-by-pixel basis. In principle, SM2RAIN parameter values could be estimated from soil texture, land use, and climatic information and from the assessment of the relative errors of SM2RAIN-based and state-of-the-art rainfall products. With the will of exploring these aspects in future studies, without loss of generality as 3B42 product is globally available, we choose to calibrate SM2RAIN parameters on gauge-corrected TMPA product.

For implementing SM2RAIN, the SMOS soil moisture data are first normalized between 0 and 1 by considering the minimum and maximum values of each pixel. Successively, normalized data are interpolated in time at 9 A.M. local time of each day. The obtained time series of relative soil moisture are used as input into the algorithm, and the four parameters (Z^{*}, a, b, and T) are calibrated by minimizing the root-mean-square error (RMSE) between the estimated rainfall and the 3B42 data set at daily time scale. The obtained rainfall product, P_{SM2RAIN}, is in turn merged with 3B42RT through equation (2) implying the calibration of k parameter; the minimization of RMSE is used also for this step. The second rainfall product is $P_{\mathrm{SM2RAIN+3B42RT}}$, for which the same procedure is applied separately for each pixel of the study area. For simplicity, the two products will be referred as SM2RAIN and SM2RAIN+3B42RT thereinafter.

2.2. API-Mod

The API-mod algorithm is based on a simple modification of the Antecedent Precipitation Index (API) initially designed to provide a proxy of the surface soil moisture with a single precipitation observation and a single parameter τ which controls the soil drying-out velocity. The API relationship can be written as

$$\mathrm{API}(t) = \mathrm{API}(t-1)\, e^{-\frac{\Delta t}{\tau}} + P(t) \tag{3}$$

A modification of the API model, API-mod, was introduced in *Pellarin et al*. [2013]. The API-mod includes two more parameters to account for soil saturation (θ_{sat}) and soil layer thickness (d_{soil}). The API-mod algorithm can be expressed as

$$\mathrm{SSM}(t) = \mathrm{SSM}(t-1)e^{-\frac{\Delta t}{\tau}} + [\theta_{\mathrm{sat}} - \mathrm{SSM}(t-1)]\left[1 - e^{-\frac{P(t)}{d\mathrm{soil}}}\right] \tag{4}$$

where θ_{sat} [L^3/L^3] is the saturated soil moisture value, d_{soil} is the soil depth [L], $P(t)$ is the rainfall accumulation [L] over a Δt period [T], and τ is a parameter which describes the soil drying-out velocity [T].

A CDF-matching procedure is done in order to avoid any bias between API-mod SSM and SMOS L3SM data. The CDF matching is a pixel-by-pixel procedure and can be expressed as

$$\mathrm{SMOS}^{\mathrm{CDF}} = p_{\,1} + p_{\,2}\ \mathrm{SMOS} \tag{5}$$

with

$$p_2 = \frac{\sigma(\text{API- mod})}{\sigma(\mathrm{SMOS})} \tag{5a}$$

$$p_1 = \mu\ \ (\text{API- mod}) - p_2\ \ \mu\ \ (\mathrm{SMOS}) \tag{5b}$$

The API-mod algorithm provides one rainfall product (Figure 1), i.e., $P_{\text{API-mod}}$, and requires the calibration of the single parameter τ on a pixel-by-pixel basis; θ_{sat} and d_{soil} parameters are assumed as spatially constant for the whole study area.

Before applying the assimilation technique, a preprocessing step is carried out to match SSM, equation (4), forced with 3B42 daily precipitation and SMOS L3SM data thus obtaining the spatial distribution of p_1 and p_2 coefficients. Then, for implementing the API-mod methodology, a particle filter assimilation scheme is used. This approach is based on stochastic perturbation of the precipitation forcing that explicitly simulates the consequence of these uncertainties in the soil moisture estimates [*Arulampalam et al*., 2002; *Doucet et al*., 2000; *Moradkhani et al*., 2005; *Van Leeuwen*, 2009]. The random generation is obtained as $K = \exp(4*\mathrm{Rand}-2)$ where Rand is a random number uniformly distributed between 0 and 1. Then, each 3 h rainfall estimate is randomly changed using the multiplicative factor K ranging from about 0.13 (e^{-2}) to about 7.3 (e^2). The assimilation time period is fixed to five successive SMOS measurements. An ensemble of 100 API-mod simulations is done, and the 10 best simulations are selected based on RMSE minimization between API-mod and SMOS soil moisture at daily time scale. The retrieval accumulation product is calculated as the mean value of the 10 best simulations (average of 10 perturbed precipitation time series). This operation is renewed for the next period of five SMOS measurements and for each 0.25° pixels of Australia. For simplicity, accumulation products $P_{\text{API-mod}}$ acquired above will be referred as API-mod thereinafter.

2.3. SMART

The Soil Moisture Analysis Rainfall Tool (SMART) [*Crow et al*., 2009, 2011] is based on the sequential assimilation of SMOS soil moisture retrievals into a daily implementation of equation (3) for the case of $P(t)$ derived from TMPA 3B42RT rainfall accumulations. For each sequential assimilation of a single SMOS retrieval, an increment of water (δ) is either added or subtracted from the analysis background in an attempt to compensate for the impact of random rainfall errors on daily API forecasts. Given their relationship to rainfall errors, these increments can be used to correct satellite-based rainfall accumulations via a simple additive correction [*Crow et al*., 2009]:

$$[P_{\mathrm{SMART}}(t)] = [P_{\mathrm{3B42RT}}(t)] + \lambda\delta \tag{6}$$

where λ is a temporally fixed (but spatially variable) constant and bracketing "[]" reflects summing within a multiday period.

The specific Kalman filter and the API model parameterization applied here follow the one described by *Crow et al*. [2011] except for three modifications. First, instead of the month-by-month approach recommended by

Crow et al. [2011], the preprocessing of SMOS surface soil moisture retrievals is based on the application of a single pixel-wise CDF-rescaling function to transform the distribution of raw SMOS retrievals to match that of the API predictions obtained from equation (3) (utilizing 3B42RT rainfall and no data assimilation). This change is made because the 4 year length of the SMOS time series is deemed too short to sample separate rescaling functions for each month. Note that this rescaling approach is similar to that described in equation (5) for API-mod, except based on the matching of all statistical moments (not just mean and variance). Second, to reflect relatively arid conditions within the Australian continent, the τ in equation (3) is lowered from the globally fixed value of -6.15 (days) recommended by *Crow et al*. [2011] to a lower value of -1.96 (days). Third, instead of applying the triple collocation-based approach recommended by *Crow et al*. [2011], soil moisture retrieval errors in assimilated SMOS soil moisture retrievals are held fixed at a constant value of 0.04 $m^3\,m^{-3}$. This ensures that the data input needs of SMART are consistent with SM2RAIN and API-mod.

A temporally constant value of λ in equation (6) is calibrated on a pixel-by-pixel basis to minimize the RMSE between $[P_{SMART}]$ and $[P_{3B42}]$ estimates (where brackets indicate either 1 day or 5 day accumulation periods). The SMART algorithm provides a single rainfall accumulation product (Figure 1), i.e., $[P_{SMART}]$. The time scale of this product is determined by the accumulation window applied in equation (6). Past experience with SMART has revealed that it is preferable to apply equation (6) using a multiday accumulation window rather than applying it at a daily time scale and *then* aggregating to a multiday period [*Crow et al*., 2009]. Therefore, in order to maximize the 5 day performance of SMART, separate implementations of equation (6), each with its own unique λ calibration, were applied to acquire 1 and 5 day SMART rainfall accumulation estimates. Note that such an approach contrasts which that of SM2RAIN and API-Mod, where 5 day accumulations were obtained by simply aggregating 1 day or 3-hourly results (see above). See below and *Crow et al*. [2011] for additional SMART implementation details. For simplicity, the $[P_{SMART}]$ rainfall accumulation products resulting from the application of equation (6) will be referred as SMART thereinafter.

2.4. Strengths and Limitations of Soil Moisture-Based Approaches

The three approaches share similar strengths and limitations. Indeed, we expect that the use of SMOS soil moisture data will have a significant impact in correcting the rainfall accumulations estimated by 3B42RT product thanks to the time-integrated look provided by soil moisture observations. However, the methods will fail in regions and conditions in which soil moisture observations are not accurate as it occurs for highly vegetated and urban areas, for regions with complex topography, and for frozen/snow soil conditions. Similarly, the methods are supposed to perform poorly when the soil is close to saturation conditions as additional rainfall, which runs directly off the surface, cannot be seen from soil moisture observations. These limitations will be more pronounced for the SM2RAIN product which is based solely on SMOS observations. For the three products integrating 3B42RT and SMOS observations (SM2RAIN+3B42RT, API-mod, and SMART), we anticipate that the overall performances are expected to improve thanks to the complementary nature of the approaches.

2.5. Performance Metrics

Three continuous metrics are used for the evaluation of the performance of the soil moisture-derived rainfall products (and TMPA products): the Pearson correlation coefficient (R), the root-mean-square error (RMSE, in mm), the mean relative error (BIAS), computed as relative error on the accumulated rainfall in the entire investigated period, the unbiased RMSE (ubRMSE, in mm), and the mean error (BIAS*, in mm), computed as the long-term mean difference. The ubRMSE is the square root of the difference between $RMSE^2$ and $BIAS^{*2}$, and it provides information regarding the random error only. Additionally, three more categorical metrics are employed: False Alarm Ratio (FAR), Probability of Detection (POD), and Threat Score (TS). FAR refers to the fraction of predicted events that are, in fact, nonevents (false positive) and POD to the fraction of all qualifying events correctly predicted; TS provides an integrated measure of the overall categorical performance. The categorical performance metrics are evaluated for different rainfall thresholds computed as rainfall percentiles (from 0 to 100°) of each pixel in the study area [e.g., *Chen et al*., 2012; *Brocca et al*., 2014].

3. Study Area and Data Sets

Precipitation across Australia is highly variable due to its significantly different climate zones, ranging from tropical in the northeast, temperate (southeastern and southwestern regions, and Tasmania), arid deserts and savannas (most of central and northern Australia), as well as semiarid regions in the transitional zones.

The rainfall pattern is therefore concentric around the extensive arid core of the continent, which generally receives only little precipitation (<60 mm/yr). The northern tropical zone experiences the majority of the annual rainfall events during the summer months (October–March), often exceeding a total depth of 2000 mm, and its winter months are dry. The tropical rain events are mainly driven by the Australian monsoon, tropical depressions, and cyclones. The southeastern midlatitude regions are temperate and have no distinctive dry season. Rain falls mostly during the warm/hot summer through low-pressure systems (e.g., the east coast low) that can bring strong storms with heavy rain, while cold frontal systems are more prominent through the cooler months. The Great Dividing Range, which runs parallel along much of the east coast, is also a likely contributor to wetter temperature summers due to its orographic influence. The southwestern regions are classified temperate but experience dry warm/hot summers (in particular from November to February). In those summer months, the west coast trough can result in large thunderstorms, provided that sufficient moist air is brought into the region. Finally, the stable and dry conditions over large parts of central Australia are attributed to the high-pressure-related subtropical ridge for most times of the year; northern arid regions can, however, occasionally receive convective rainfall during periods of monsoon and depressions in the tropics.

3.1. AWAP Data Set

The AWAP rainfall product is generated via spatial analyses on the quality-controlled daily rain gauge measurements from the Australian Bureau of Meteorology daily rain gauge network (accessed online via http://www.bom.gov.au/jsp/awap/rain/archive_recal.jsp). The first analysis method applied to daily anomalies (given by the ratio of daily rainfall to monthly mean) is based on a two-dimensional Barnes successive correction technique that interpolates point-gauge data by applying a weighted averaging process. Second, the three-dimensional (i.e., latitude, longitude, and altitude) smoothing splines are used for the analysis of monthly climatological averages of rainfall. Both methods generate analysis fields that achieve their smallest errors subject to constraints on the smoothness and the spectrum of the final field. The analysis fields from the anomaly and climatology analyses are combined via simple multiplication. To reduce biases in daily estimates at this step, the daily rainfall analyses are recalibrated so that their sum is equal to the monthly rainfall analyses. AWAP daily rainfall for a given day is the 24 h total rainfall from local time 9 A.M. the day before to 9 A.M. the current day. The rainfall fields are gridded on a $0.05° \times 0.05°$ grid and spatially resampled to the desired $0.25° \times 0.25°$ grid by taking area-weighted averages.

This product has known shortcomings [e.g., *Contractor et al.*, 2015]. The network has a varying density across the country (and also varies with time), with a strong focus on the urbanized coastal areas along the east, southeast, and southwest, while the network is extremely sparse in central Australia and essentially nonexistent in the barely populated central west. The accuracy of the data varies considerably across Australia (with higher analysis errors in the northern tropics than other regions), since it is limited to what can be resolved by the station network. In central Australia, the network is too sparse to support a daily rainfall analysis, leading to the data "voids" in Figure 2, which is considered acceptable, due to the little rainfall occurring in those regions. While the analysis errors tend to increase away from the gauges, the errors also tend to increase in data-rich areas such as in southeast Australia and in regions with strong rainfall gradients and/or with significantly orography; the spatial analysis can lead to smoothing such that grid point values may differ slightly from the exact reading at the contributing stations. The daily spatial analysis of highly convective systems, which are short and variable in length scales in the tropics, is clearly more susceptible to errors due to data smoothing, variability of the Barnes parameters, and the station network density. While the AWAP analysis typically underestimates intensity and frequency of extreme rainfall events, the intensity and frequency of low rainfall events are typically overestimated. On the whole, the mean average error is about 50% of the average daily rainfall, based on cross-validation analysis [*Jones et al.*, 2009]. For this study we have masked out the pixels where AWAP contains fewer than 50% of total 1461 analysis days (see Figure 2).

3.2. Satellite Data Sets

For the SMOS data set [*Kerr et al.*, 2012], the reprocessed level 3 (L3) data generated with the version 5.51 of the algorithm are taken. The L-Band Microwave Emission of the Biosphere Model [*Wigneron et al.*, 2007] is used for inverting SM from dual-polarized multiangular brightness temperature observations of SMOS; the algorithm details can be found in *Kerr et al.* [2012]. The product is expressed in volumetric terms (m^3/m^3) and is representative of a soil layer of about 3.5 cm. The product is available from January 2010 with a spatial

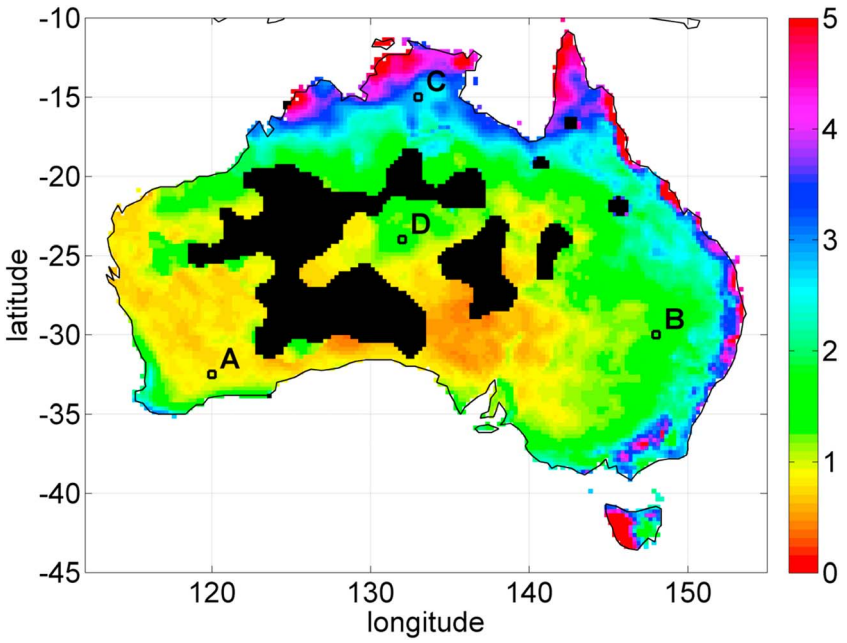

Figure 2. Climatology of the study area expressed as mean daily rainfall rate (mm/d) in the investigated period (from 15 January 2010 to 30 November 2013) obtained by the AWAP data set. The four letters indicate the 1° boxes for which the monthly rainfall time series are shown in Figure 5. Black areas represent the zones in which AWAP data are not available.

sampling of 0.25°. We note here that the analysis was carried out also with the new SMOS product (version 6.20), only with SM2RAIN, but no significant differences in the results are found. Therefore, we finally decided to use version 5.51 SMOS product. We also underline that in the period January–June 2010 the SMOS data are expected to be of lower quality due to the commissioning phase but removing this period did not have a significant impact on results and hence we preferred to consider the longer period.

The real-time (3B42RT) and the gauge-corrected version 7 (3B42) TMPA products, developed by *Huffman et al*. [2007], are used in this study. The TMPA algorithm combines infrared information from geosynchronous satellites and several microwave precipitation estimates from active and passive microwave sensors. The 3B42 product is bias adjusted to the monthly Global Precipitation Climatology Centre gauge analyses [*Schamm et al*., 2013]. The real-time product does not include any ground-based information. The TMPA products have coverage of 50°N–50°S and are produced at the 3 h/0.25° temporal/spatial resolution. The accumulated daily rainfall is obtained by aggregating the eight 3 h time windows every day. It should be noted that TMPA data are provided within a time window ±90 min from the nominal time (0000, 0300, …, 2100 UTC), while the satellite soil moisture product and the observed rainfall data set are delivered in local time, i.e., UTC + 9 (on average over Australia). Therefore, the daily accumulated rainfall product from 3B42 and 3B42RT represents the total rainfall starting, and ending the next day, at 07:30, with 1.5 h of delay with respect to the other products.

4. Results

In the following section, the details of the three different methods applied across Australia are presented together with the corresponding results. First, the values of the parameters of each method are reported, and then the continuous and categorical assessment of the obtained rainfall product is described at different temporal scales (1 day, 5 days, and monthly).

4.1. Parameter Values of Rainfall Estimation Algorithms

Following the procedure described in section 2, the parameter values of each method are computed by using 3B42 as benchmark. Table 1 shows the summary statistics of the spatial distribution (median, standard deviation, and 25th and 75th percentiles) of each parameter that is considered to be varying in space for each

Table 1. Summary Statistics of the Spatial Distribution of the Calibration Parameters of Each Method; See Text for the Definition of Symbols (σ: Standard Deviation; 25th and 75th: Percentiles)[a]

Parameters		Z^* (mm)	a (mm d^{-1})	b (−)	T (Day)	k (−)
SM2RAIN	median	77.2	11.5	5.3	2.9	0.25
	σ	135.3	26.9	17.5	6.8	0.18
	25th	48.2	0.0	2.1	1.5	0.11
	75th	125.3	23.4	27.3	6.6	0.38
Parameters		τ(hours)				
API-mod	median	209.2				
	σ	45.4				
	25th	174.0				
	75th	262.3				
Parameters		λ (1 day) (−)	λ (5 days) (−)			
SMART	median	0.15	0.30			
	σ	0.14	0.19			
	25th	0.09	0.21			
	75th	0.23	0.41			

[a]Note that the SMART algorithm requires separate calibration parameters for 1 and 5 day accumulation results.

method. The percentiles are computed on the obtained parameter values and aim at providing an estimate of the frequency distribution of their spatial variability.

The strategy for the parameterization of each method is different. For SM2RAIN and SMART, the parameter values are calibrated based on the explicit minimization of errors (RMSE) with respect to 3B42 retrievals. Specifically, as mentioned above, two separate calibrations are carried out with SMART for 1 day and 5 day rainfall correction. For API-mod, the single parameter τ is parameterized as a function of soil texture information instead of performing a pixel-by-pixel calibration.

For SM2RAIN, the obtained parameter values are quite consistent with those of previous studies by *Brocca et al*. [2014] and *Ciabatta et al*. [2015], despite that the application of the exponential filter was not used in those studies. In particular, the Z^* parameter is found to be higher than in previous investigations likely due to the application of the exponential filter. Indeed, the filter smooths the soil moisture signal, which in turn becomes representative of a thicker soil layer thus increasing Z^*value. Similar considerations can be made for the other parameters. The spatial variability of the parameter values resembles the one found in *Brocca et al*. [2014] and *Ciabatta et al*. [2015] as higher Z^* for higher rainfall rates (i.e., northern and eastern Australia; see Figure 2) and higher a values along the coasts where the SMOS signal is more noisy [*Ciabatta et al*., 2015].

For the API-mod methodology, similarly to previous studies [*Pellarin et al*., 2013; *Louvet et al*., 2015], soil depth (d_{soil}) is fixed to 100 mm and θ_{sat} is fixed to 0.41 m^3 m^{-3}, whereas τ is assumed to be related to clay fraction as $\tau = 32\ \ln(\text{clay}) + 174$ with clay ranging from 0 to 100% [*FAO/IIASA/ISRIC/ISSCAS/JRC*, 2012]. Thus, only three parameters are spatially distributed over Australia in the API-mod method (p_1, p_2, and τ; see equations (4) and (5)).

SMART requires calibration of a single parameter λ used to convert the Kalman increment of API into a corrective precipitation increment. However, values of optimized λ have a complex relationship with the accumulation time scale applied in equation (6) [*Crow et al*., 2009]. Therefore, as discussed above, calibrated λ values are obtained separately for individual accumulation time scales [*Crow et al*., 2009]. Table 2 shows optimized λ results obtained for both 1 and 5 day accumulation results. Relative larger 5 day λ results reflect tendency for rainfall-induced soil moisture signals to dampen over time. Since SMART is run assuming no spatial heterogeneity in SMOS soil moisture retrieval errors, spatial patterns in calibrated values of λ (not shown) tend to reflect the reduced reliability of SMOS-based updates over densely vegetated areas. That is, lower values of λ are found in areas of higher biomass (and vice versa).

4.2. Performance Assessment

In this section, the capability of reproducing different features of observed rainfall is described for each algorithm (e.g., bias, temporal dynamic, and occurrence), along with their strengths and weaknesses.

Table 2. Summary Statistics of the Spatial Distribution of Performance Scores of the Different Satellite Rainfall Products in the Comparison With AWAP Data[a]

		1 Day Rainfall			5 Day Rainfall				
Product		R	RMSE (mm)	TS	R	RMSE (mm)	TS	BIAS (−)	|BIAS| (−)
3B42	10th	0.53	3.06	0.30	0.67	6.48	0.53	−0.14	0.02
	50th	0.68	4.73	0.42	0.80	10.70	0.66	0.03	0.09
	90th	0.78	8.69	0.54	0.88	20.08	0.76	0.21	0.25
3B42RT	10th	0.46	3.44	0.27	0.54	8.30	**0.48**	**−0.18**	0.05
	50th	0.62	5.59	**0.40**	0.71	14.00	0.62	0.20	0.26
	90th	0.73	9.44	**0.52**	0.83	24.04	0.74	0.70	0.72
SM2RAIN	10th	0.40	**2.61**[d]	0.27[c]	0.58[c]	**6.04**[d]	0.46	−0.26	**0.02**[d]
	50th	0.56	4.40[d]	0.38	0.74[c]	**10.71**[c]	0.60	**0.01**[d]	**0.12**[c]
	90th	0.66	8.50[d]	0.48	0.83[c]	23.37[c]	**0.81**[d]	**0.27**[c]	**0.37**[c]
SM2RAIN+ 3B42RT	10th	**0.51**[b,c]	2.86[d]	**0.28**[c]	0.61[b,c]	6.81[c]	0.47	**−0.18**[c]	0.04[c]
	50th	**0.65**[b,c]	**4.39**[d]	**0.40**[c]	**0.76**[b,c]	11.07[c]	0.60	0.15[c]	0.20[c]
	90th	**0.75**[c]	**8.16**[d]	**0.52**[c]	**0.85**[c]	**20.72**[c]	0.78[d]	0.47[c]	0.53[c]
API-mod	10th	0.44	3.29[c]	0.24	0.57[c]	6.57[c]	0.47	−0.21	0.03[c]
	50th	0.58	5.43[c]	0.37	0.73[c]	11.89[c]	0.61	0.07[c]	0.15[c]
	90th	0.69	9.03[c]	0.48	0.83[c]	22.20[c]	0.72	0.37[c]	0.42[c]
SMART	10th	0.48[c]	3.16[c]	**0.28**[c]	**0.62**[b,c]	6.77[c]	**0.48**[c]	−0.24	0.03[c]
	50th	0.63[c]	5.24[c]	0.39	**0.76**[b,c]	12.13[c]	**0.63**[c]	0.09[c]	0.18[c]
	90th	0.74[c]	9.04[c]	0.50	**0.85**[c]	22.53[c]	**0.81**[d]	0.50[c]	0.59[c]

[a]The best performance of each metric is reported in bold for products based only on satellite data (except 3B42). R: Pearson's correlation coefficient; RMSE: root-mean-square error, TS: Threat Score for a rainfall threshold of 0.2 mm; BIAS: mean error; |BIAS|: absolute BIAS; 10th, 50th, and 90th: percentiles.
[b]R values of SMOS estimated/corrected products are significantly different from 3B42RT at a significance level of 0.10 (one-tailed test).
[c]The scores better (≥) than the real-time TMPA product 3B42RT.
[d]The scores better (≥) than the gauge-corrected TMPA product 3B42.

4.2.1. Continuous Scores

Continuous performance scores (*R* and RMSE) are computed for both 1 day and 5 day accumulated rainfall, and the summary statistics of their spatial distribution are given in Table 2. Specifically, all the performances are referred to the comparison with the AWAP data set, and six different satellite-based rainfall products are analyzed: 3B42, 3B42RT, SM2RAIN, SM2RAIN+3B42RT, API-mod, and SMART. As in Table 1, the percentiles are simply computed on the values obtained for each performance score and aim at providing an estimate of their frequency distribution. The performance of 3B42 is reported here as a baseline product. However, we note that 3B42, by retrospectively including ground-based observations, is not comparable with the other products based solely on near-real-time satellite observations. The top down baseline to be compared with SMOS-based rainfall products is the (purely remotely sensed) 3B42RT product. Additionally, the SM2RAIN product should be analyzed separately from the other three products (SM2RAIN+3B42RT, API-mod, and SMART) as it considers only SMOS soil moisture data and does not utilize 3B42RT rainfall improvement. As there is an extreme range of precipitation patterns across Australia, the performances are also computed for each climatic zone. The relative comparison between these zone-specific scores is quite similar to that obtained for the whole Australia with only minor differences (outlined below) and, hence, not shown here for brevity.

In terms of correlation, which provides information about the ability of reproducing the relative temporal dynamics of observations, 3B42RT performs quite well for both 1 day and 5 day accumulated rainfall with median *R* values equal to 0.62 and 0.72, respectively. SM2RAIN provides lower (higher) scores for 1 day (5 day) accumulated rainfall. Indeed, as shown in previous studies [e.g., *Brocca et al*., 2014], the revisit time of SMOS observations (~2 days in Australia) is not suitable for accurately estimating rainfall at daily time scale. Nevertheless, both SM2RAIN+3B42RT and SMART are found to outperform 3B42RT with consistent results, which are also close to those of 3B42. For SM2RAIN+3B42RT (SMART) the median *R* values are equal to 0.65 (0.63) and 0.76 (0.76) for 1 day and 5 day accumulated rainfall, respectively, and these values are significantly different from those obtained with 3B42RT (significance level of 0.10, one-tailed test). The performance of API-mod is found to be slightly lower in terms of correlation, specifically for 1 day rainfall estimates. The spatial distribution of the local correlations is shown in Figure 3 for 1 day and 5 day accumulated rainfall. Figure 3 (left column) represents the correlation maps obtained with 3B42RT, and Figure 3 (right column) presents the ratio between the correlations obtained with SMOS-based products and the baseline (3B42RT). Therefore, from Figure 3 (left column) the spatial pattern of the performance is shown, while

Figure 3 (right column) provides an immediate understanding of the areas where an improvement (blue) and a deterioration (red) of performances occur. For 1 day rainfall it is evident that SM2RAIN+3B42RT and SMART provide a significant improvement of the correlation, mainly in the central part of Australia (arid climate). SM2RAIN and API-mod have lower performance, and only by considering 5 day accumulated rainfall, a widespread improvement related to these two products is observed. Interestingly, the lower performance of the SMOS-based rainfall products is found along the coast and particularly in the southeastern (temperate climate) part of Australia (evident for SM2RAIN at 1 day). This region is characterized by a high density of vegetation and the presence of urban areas, and, hence, the lower accuracy of SMOS soil moisture product is expected.

In terms of RMSE (see Table 2), which aims at characterizing the random error plus the BIAS between observed and estimated rainfall data, the relative performances of the products are different with respect to correlations. The baseline 3B42RT product has quite large RMSE values (e.g., median RMSE = 5.59 mm for 1 day rainfall), partly due to the tendency to overestimate observations (median BIAS = 0.20). Therefore, all SMOS-based rainfall products outperform 3B42RT for both rainfall accumulations. The best performing products are SM2RAIN +3B42RT for 1 day accumulation and SM2RAIN for 5 day accumulations. Interestingly, for 1 day rainfall SM2RAIN-related products show performance scores even better than the gauge-corrected 3B42. Differently from the correlations, API-mod provides comparable scores with SMART. The absolute BIAS (last column of Table 2) gives nearly the same picture of RMSE with all the SMOS-based products outperforming 3B42RT and the best results for SM2RAIN. Figure 4, similarly to Figure 3, shows on the spatial distribution of RMSE values obtained through 3B42RT (left column) and the improvement (blue)/deterioration (red) that is found due to the use of SMOS soil moisture data for rainfall estimation/correction (right column). Clearly, all the maps highlight that the use of SMOS largely improves the estimation of rainfall in terms of RMSE, with all the products providing the largest added value in central Australia (arid climate). The overall spatial patterns of RMSE and *R* values are in good agreement (e.g., low to no improvement along the coast and better scores in central Australia).

In the supporting information, we have also decomposed RMSE into ubRMSE and BIAS* components to examine the individual contributions of mean error and random and multiplicative errors. Figures S1 and S2 show, similarly to Figure 4, the spatial distribution of ubRMSE and BIAS* (in absolute terms), respectively, for 3B42RT product and the relative performances of each SMOS-derived rainfall product with respect to 3B42RT. It is evident that random error is the major component of the total difference between AWAP and satellite-derived data sets (i.e., ubRMSE is much higher than BIAS*). Therefore, the results of RMSE and ubRMSE are qualitatively the same. In terms of BIAS* an overall improvement is observed for all products with higher improvements/deteriorations for SM2RAIN and API-mod products and lower differences for SM2RAIN +3B42RT and SMART. As for RMSE, the spatial distribution and the impact of SMOS-derived rainfall product are very similar if 1 day and 5 day rainfall accumulations are considered.

In Figure S3 in the supporting information, the performance scores are grouped by rainfall intensity (computed based on the AWAP data set). Specifically, data are grouped in drizzle (rainfall $\leq$5 mm/d), moderate rainfall (5–15 mm/d), and heavy rainfall ($\geq$15 mm/d) events. As expected, the larger improvements in the results (e.g., higher *R* and lower ubRMSE) are obtained for low-intensity rainfall events ($<$15 mm), even though small improvements are made also for heavy rainfall event by SM2RAIN+3B42RT and SMART. In terms of random error (ubRMSE), SM2RAIN product shows distinctively lower values than the other products. This aspect should be related to the tendency to underestimate rainfall of SM2RAIN (see BIAS* results), particularly important for moderate and heavy rainfall events. Generally, for all products drizzle rainfall events are slightly overestimated, whereas heavy rainfall events are underestimated (moderate rainfall events have nearly no BIAS*, except SM2RAIN).

Moreover, the impact of seasonality on the performance is analyzed by computing the performance scores for different seasons (Figure S4). The performance varies with seasons without presenting specific patterns. Therefore, we conclude that seasonality does not have a significant impact on the products' accuracy.

Performance scores are also computed as a function of soil saturation (not shown) obtained by SMOS. Results do not show a clear pattern with similar performances for different soil moisture levels and also for close to saturation conditions. At the spatial resolution investigated in this study (25 km), complete spatial saturation is rare, and, hence, the saturation problem has a low relative impact on results. However, further investigations specifically dedicated to this aspect are needed in order to assess at what spatial resolution the saturation problem becomes significant.

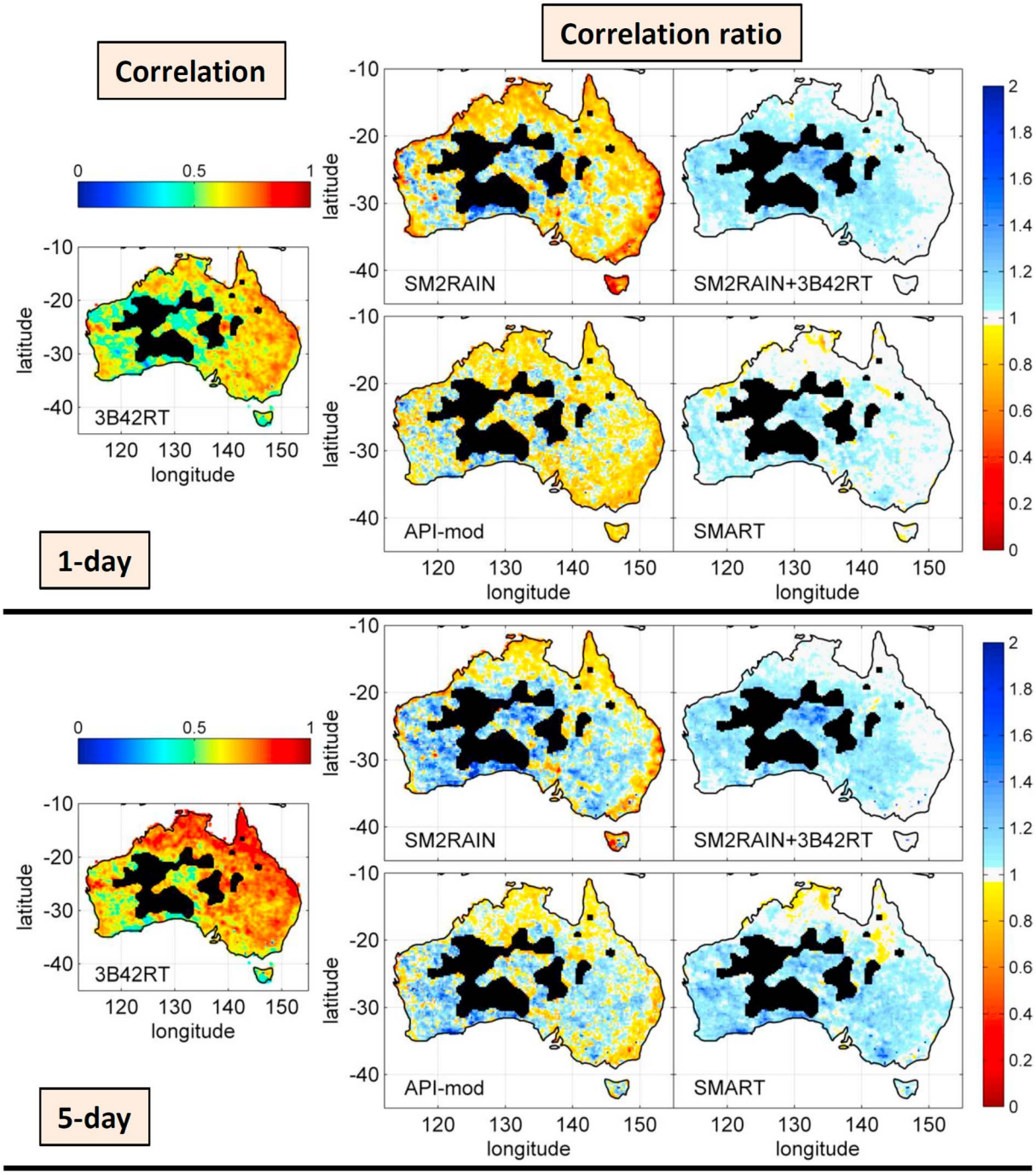

Figure 3. (left column) Pearson's correlation maps between AWAP-observed accumulated rainfall and TMPA 3B42RT product. (right column) Correlation ratio maps between the correlation obtained by comparing the four different SMOS-derived products (SM2RAIN, SM2RAIN+3B42RT, API-mod, and SMART) with AWAP-observed rainfall and the correlation obtained with TMPA 3B42RT (Figure 3, left column); red pixels indicate degradation (lower correlations), whereas blue pixels an improvement (higher correlations). The analysis period is from 14 January 2010 to 30 November 2013, and the top (bottom) rows show results for 1 day (5 day) accumulated rainfall. Black areas represent the zones in which AWAP data are not available.

4.2.2. Categorical Scores

Besides the continuous performance scores, rainfall products should be analyzed in terms of their capacity to detect the occurrence of rainfall events. In Table 2 the summary statistics of the TS values are given for each product. TS integrates POD and FAR scores and is computed in Table 2 for a rainfall threshold of 0.2 mm. 3B42RT provides quite accurate results with median TS values equal to 0.40 and 0.62 for 1 day and 5 day

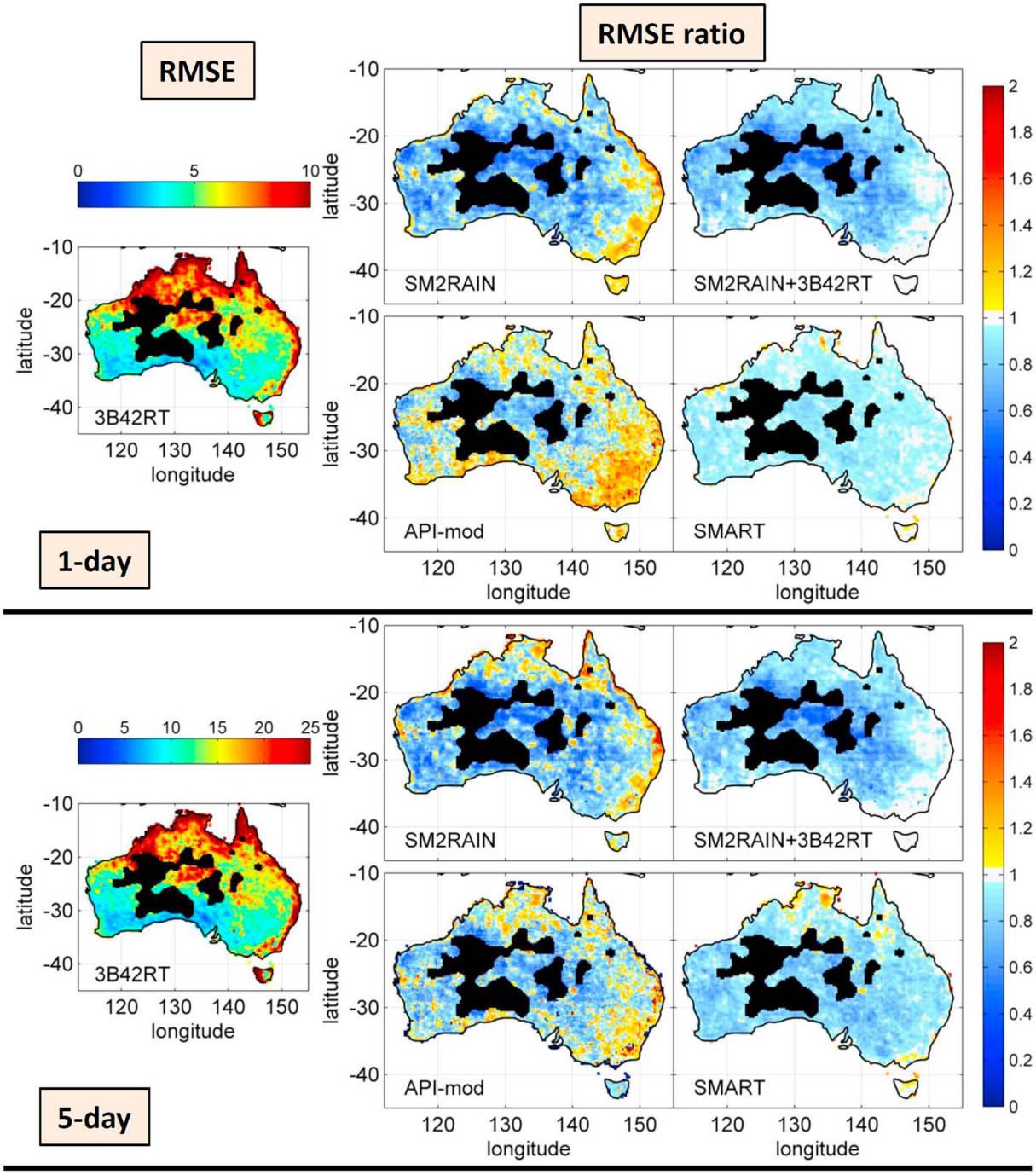

Figure 4. As in Figure 3 but for the root-mean-square error (RMSE). Red pixels indicate degradation (higher RMSE), whereas blue pixels indicate an improvement (lower RMSE). Note that the color bar is inverted with respect to Figure 3.

accumulated rainfall, respectively. SMOS-based products generally provide equal or lower performances with the SM2RAIN+3B42RT product giving the best scores for 1 day accumulated rainfall. For 5 day rainfall, SMART has the best scores (except for the 10th percentiles) with median TS of 0.63.

Figure 5 shows the POD, FAR, and TS values in each panel for both 1 day and 5 day accumulated rainfall. Plots show the median (±1 standard deviation) values of each categorical score and for different rainfall threshold computed as the 10th, 50th, and 90th percentiles of the AWAP-observed rainfall in each pixel. Therefore, the panels show the capability of the products to detect rainfall occurrence for low to high rainfall events (from left

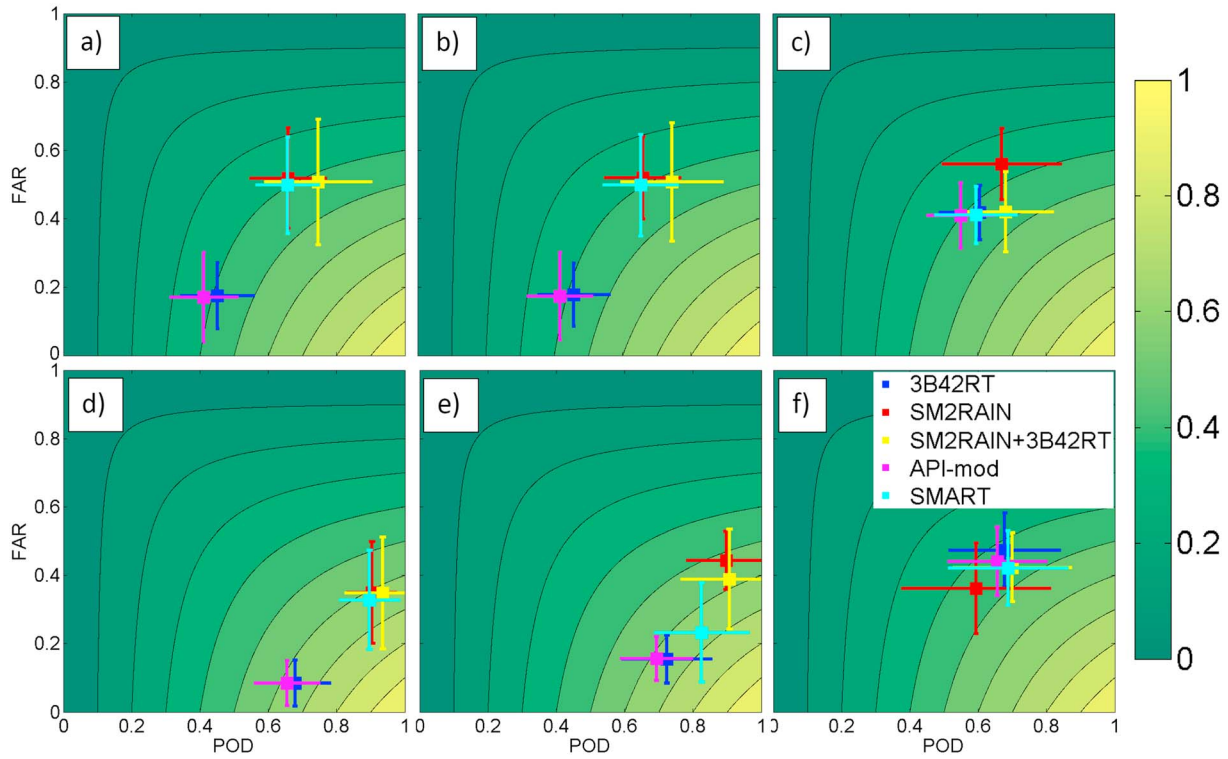

Figure 5. POD (Probability of Detection) versus FAR (False Alarm Ratio) plots for (a, d) 10th, (b, e) 50th, and (c, f) 90th percentile and for 1 day (Figures 5a–5c) and 5 day (Figures 5d–5f) accumulated rainfall. The contour lines indicate TS (Threat Score) values, the horizontal (vertical) bars represent the standard deviation of POD (FAR), and the square is the median value. Squares represent the median POD (FAR) over all pixels for the 10th, 50th, and 90th percentiles at that pixel. Optimal performances are for FAR = 0, POD = 1, and TS = 1. Percentiles represent the rainfall threshold used for the computation of the scores. Therefore, low (high) percentiles indicate the product capability to detect high (low) rainfall intensities.

to right). For 1 day rainfall (Figures 5a–5c), SM2RAIN and API-mod give the lower performance in terms of TS. SMART, SM2RAIN, and SM2RAIN+3B42RT have a quite high probability of falsely identifying rainfall events (high FAR) but a good detection capability (high POD). 3B42RT and API-mod have an opposite behavior with low FAR and relatively low POD values. It should be also underlined that for 90th percentiles (high rainfall intensities) the product's behavior is more similar and the best product is found to be SM2RAIN+3B42RT. For 5 day rainfall (Figures 5d–5f), the product's performance is better (lower FAR and higher POD) but with a similar patterns of 1 day rainfall. For medium to high rainfall intensities (50th and 90th percentiles, 5 day rainfall), the best product is SMART with values very close to the optimal performance (FAR = 0, POD = 1, TS = 1) for the 50th percentiles. Overall, performances deteriorate from left to right mainly due to the increased difficulty of detecting high-intensity rainfall events. The overall performance of SMOS-based rainfall products are in agreement with previous studies by *Chen et al*. [2012], *Brocca et al*. [2014], and *Ciabatta et al*. [2015] who found that the soil moisture correction improves POD and deteriorates FAR, with a corresponding slight increase in TS.

Figure S5 in the supporting information shows the spatial distribution of TS values for 3B42RT product and the relative performances of each SMOS-derived rainfall product with respect to 3B42RT. A rainfall threshold of 0.2 mm (1 day rainfall) and 1 mm (5 day rainfall) is considered. Interestingly, these maps show different spatial patterns with respect to *R* and RMSE. For SM2RAIN, SM2RAIN+3B42RT, and SMART, improvements in the performances are obtained in southern and eastern Australia, while deterioration is noticeable over central and northern Australia. API-mod shows a slight deterioration throughout the continent for 1 day rainfall and a nearly neutral impact for 5 day rainfall. These results clearly indicate that the improvements obtained for *R* and RMSE in previous analyses do not convey over to categorical rainfall detection, likely due to the good performance of 3B42RT product in this respect.

4.2.3. Monthly Scale Analysis

The temporal pattern of observed (AWAP) and estimated (SMOS-based) rainfall is analyzed for the four 1° domains identified in Figure 2. In particular, Figure 6 shows monthly rain time series of all products (5 day

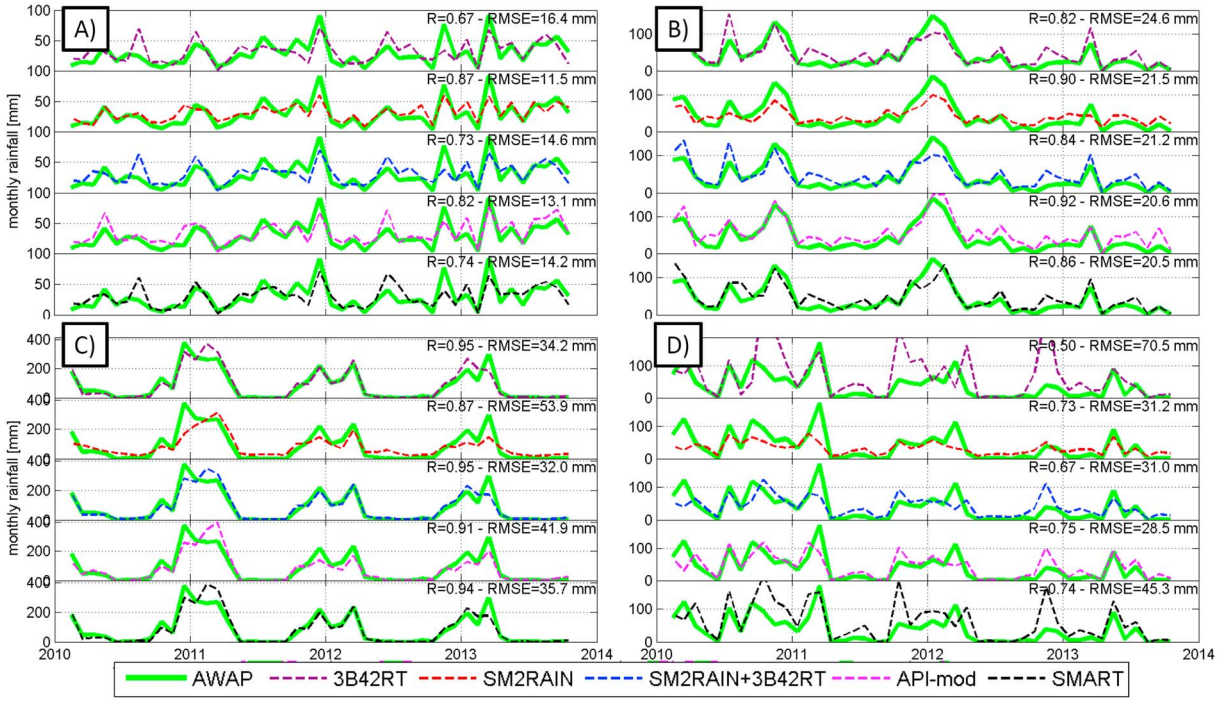

Figure 6. Time series of monthly rainfall obtained from observations (AWAP), the real-time TMPA product (3B42RT), and the SMOS-derived products (SM2RAIN, SM2RAIN+3B42RT, API-mod, and SMART) for the four boxes shown in Figure 2 (*R*: Pearson's correlation coefficient; RMSE: root-mean-square error).

SMART simulation are considered here). The main purpose of Figure 6 is to visualize explicitly the capability of the different rainfall products to reproduce the total volume of rainfall, while a corresponding figure at daily time scale is reported in the supporting information (see Figure S6) to show the products' performance in reproducing short-term fluctuations. The agreement with observations at monthly time scale is very good for all products with the exception of SM2RAIN in Figure 6c (underestimation) and 3B42RT and SMART in Figure 6d (note that these differences are not clearly visible at daily time scale, Figure S6). The figures highlight that the temporal dynamic of SMART and 3B42RT is very similar (e.g., Figure 6d), while the other three SMOS-based products (SM2RAIN, SM2RAIN+342RT, and API-mod) are more independent from 3B42RT. Overall, by analyzing the *R* and RMSE scores at monthly time scale (not shown for brevity), the SMOS-based products performance is very good (median $R > 0.80$); API-mod, SM2RAIN, and SM2RAIN+342RT provide the lowest RMSE (median RMSE ~ 31.3 mm) in agreement with results shown in Table 2. 3B42RT shows slightly lower scores for correlations (median $R = 0.77$) but significantly higher RMSE values (39 mm). At daily time scale (Figure S6), the same relative performances are obtained. SM2RAIN+342RT and SMART products consistently achieve the best scores for the four boxes.

5. Discussion

The most evident result is that all the SMOS-based products have lower RMSE values than the retrospective 3B42RT product and in some cases even better than the gauge-corrected 3B42 product. This result highlights the importance of using satellite soil moisture data as a fully independent source of information that can be effectively used for correcting the cumulative error of state-of-the-art, near-real-time rainfall products. Indeed, state-of-the-art rainfall products are affected by the structural error of undersampling rainfall in time due to the instantaneous nature of the retrieval approaches. Soil moisture data are able to correct exactly this type of error thus providing a more accurate assessment of the accumulated rainfall in near real time as testified by a significant reduction of RMSE (e.g., >25% for SM2RAIN+3B42RT product; see Table 2).

However, there are differences in the algorithm performances. Specifically, the SM2RAIN+3B42RT product seems to slightly outperform the other three products (SM2RAIN, API-mod, and SMART) likely due to the heavier calibration procedure. SM2RAIN estimates rainfall from soil moisture data only; thus, it is able to

partly correct, and even replace, the deficiencies of the top down rainfall product (e.g., due to the missing of rainfall event). Therefore, SM2RAIN is highly sensitive to the quality of the soil moisture observations and their temporal resolution (for SMOS is about 2 days in Australia) and, if not integrated with 3B42RT (i.e., with SM2RAIN+3B42RT), performs slightly worse than the other rainfall products. Differently, SM2RAIN+3B42RT, API-mod, and SMART are conceived as correction approaches, and hence, they have a stronger reliance on satellite rainfall product. For instance, API-mod is based on multiplicative factors (that are theoretically better than additive factors) for correcting rainfall and, hence, it is not able to add rainfall if the state-of-the-art product is equal to zero. SMART also requires rainfall input to predict proxy soil moisture via the API model; however, missing rainfall values can be assumed to be zero and corrected by the SMART analysis and by SM2RAIN+3B42RT.

We also highlight that the good performance obtained in this study, particularly with SM2RAIN-based products, is due to the high quality of SMOS soil moisture data in Australia and also to their relatively finer temporal resolution (i.e., frequent overpasses) with respect to other locations worldwide. We expect that the results might significantly change if these two conditions will not be fulfilled. A global-scale analysis will be the object of future investigations to provide information to this point.

6. Conclusions

In this study, the comparison of three different methods exploiting satellite soil moisture observations for improving near-real-time remote sensing of rainfall is compared over the Australian continent and by considering the SMOS soil moisture product in a 4 year period (2010–2013). The overall results highlight that the three proposed methods (SM2RAIN [*Brocca et al*., 2014], API-mod [*Pellarin et al*., 2013], and SMART [*Crow et al*., 2011]) improve the performance of the state-of-the-art (3B42RT) product in terms of both continuous (Figures 3 and 4, S1–S4, and Table 2) and categorical scores (Figures 5 and S5) and at different temporal scales from daily to monthly (Figures 6 and S6). These promising results open a number of opportunities for further improving our capability for estimating near-real-time rainfall exclusively from remote sensing.

First, this study considers only a single satellite soil moisture product (SMOS). The reasoning behind the estimation/correction of rainfall by using soil moisture data is based on the positive differences in soil moisture after rainfall pulses. Therefore, it is evident that increasing the temporal resolution of soil moisture observations, (1) a higher resolution rainfall product (e.g., 3-hourly) can be obtained and (2) higher accuracy, thanks to a better sampling of rainfall temporal variability, can be achieved. Besides SMOS, other accurate and mature satellite soil moisture products are currently available (SMAP—Soil Moisture Active and Passive mission, ASCAT—Advanced SCATterometet, and AMSR2—Advanced Microwave Scanning Radiometer 2) and their merging is an obvious continuation of this research activity.

Second, the improvement of the algorithms used here is another important point to be investigated. Specifically, the Land Surface Model used in the three algorithms is quite simplified and does not take into account certain hydrological processes (e.g., the vertical and horizontal movement of water in the soil) that might play an important role for the estimation of rainfall. The European Space Agency-funded project SMOS +rainfall will be dedicated to perform a detailed scientific analysis of the different algorithms in well-gauged areas in order to expand the knowledge of their limitations and provide suggestions for their improvement (if possible). Specifically, it is expected that a more complex Land Surface Model might improve the detection capability of the algorithms (e.g., high FAR for SM2RAIN and SMART and low POD for API-mod, Figure 6) with a better characterization of the relationship between soil moisture and rainfall as a function of rainfall intensity.

Third, we emphasize that this work should be considered as a precursor study to apply the methods to GPM products that are expected to be of higher quality than TMPA. For instance, the integration of SMAP-derived rainfall product and GPM products will be the object of future investigations. We also note that the quasi-global availability of both TMPA (±50°) and GPM (early and late run, ±60°) products allows to easily extrapolate the adopted approaches to other regions. Additionally, the procedure can be implemented in near real time due to the recent availability of SMOS [*Rodriguez-Fernandez et al*., 2015], and others, soil moisture products with a latency of a few hours. The corresponding high-quality satellite-based rainfall product can be extremely helpful in many applications such as the mitigation of natural hazards (e.g., floods and landslides) that needs accurate rainfall estimates in near real time and over large areas.

Finally, there is the need to perform the analysis on a global scale and at high spatial resolution (~25 km) as in this study. Indeed, the methodologies can be easily exported on a global scale thanks to the global availability of TMPA and, currently, GPM products. The final assessment of soil moisture-based rainfall products needs, on the one hand, an implementation worldwide and, on the other hand, a testing in hydrological, climatic, and agricultural applications. These studies will be carried out in the near future for providing a comprehensive assessment of the potential (and the limitations) of the new bottom up approach illustrated here.

Acknowledgments

We would like to acknowledge the Australian Bureau of Meteorology for providing daily rainfall data (accessed online via http://www.bom.gov.au/jsp/awap/rain/archive_recal.jsp), the support of the European Space Agency SMOS+rainfall project (contract 4000114738/15/I-SBo), and of the Centre National d'Etudes Spatiales TOSCA. SMOS L3SM product was provided by the Centre Aval de Traitement des Données SMOS (CATDS), developed by CNES in collaboration with CESBIO and IFREMER. All the input data sets used in the paper are available for free through public websites. The four rainfall products estimated/corrected by using SMOS soil moisture data are available upon request from the corresponding author.

References

Al-Yaari, A., et al. (2014a), Global-scale evaluation of two satellite-based passive microwave soil moisture datasets (SMOS and AMSR-E) with respect to Land Data Assimilation System estimates, *Remote Sens. Environ.*, *149*, 181–195.

Al-Yaari, A., et al. (2014b), Global-scale comparison of passive (SMOS) and active (ASCAT) satellite based microwave soil moisture retrievals with soil moisture simulations (MERRA-Land), *Remote Sens. Environ.*, *152*, 614–626.

Arulampalam, M. S., S. Maskell, N. Gordon, and T. Clapp (2002), A tutorial on particle filters for online nonlinear/non-Gaussian Bayesian tracking, *IEEE Trans. Signal Process.*, *50*, 174–188.

Brocca, L., T. Moramarco, F. Melone, W. Wagner, S. Hasenauer, and S. Hahn (2012), Assimilation of surface and root-zone ASCAT soil moisture products into rainfall-runoff modelling, *IEEE Trans. Geosci. Remote Sens.*, *50*(7), 2542–2555.

Brocca, L., F. Melone, T. Moramarco, and W. Wagner (2013), A new method for rainfall estimation through soil moisture observations, *Geophys. Res. Lett.*, *40*, 853–858, doi:10.1002/grl.50173.

Brocca, L., L. Ciabatta, C. Massari, T. Moramarco, S. Hahn, S. Hasenauer, R. Kidd, W. Dorigo, W. Wagner, and V. Levizzani (2014), Soil as a natural rain gauge: Estimating global rainfall from satellite soil moisture data, *J. Geophys. Res. Atmos.*, *119*, 5128–5141, doi:10.1002/2014JD021489.

Brocca, L., C. Massari, L. Ciabatta, T. Moramarco, D. Penna, G. Zuecco, L. Pianezzola, M. Borga, P. Matgen, and J. Martínez-Fernández (2015), Rainfall estimation from in situ soil moisture observations at several sites in Europe: An evaluation of SM2RAIN algorithm, *J. Hydrol. Hydromech.*, *63*(3), 201–209.

Chen, F., W. T. Crow, and T. H. Holmes (2012), Improving long-term, retrospective precipitation datasets using satellite-based surface soil moisture retrievals and the soil moisture analysis rainfall tool, *J. Appl. Remote Sens.*, *6*(1), 063604.

Ciabatta, L., L. Brocca, C. Massari, T. Moramarco, S. Puca, A. Rinollo, S. Gabellani, and W. Wagner (2015), Integration of satellite soil moisture and rainfall observations over the Italian territory, *J. Hydrometeorol.*, *16*(3), 1341–1355.

Ciabatta, L., L. Brocca, C. Massari, T. Moramarco, S. Gabellani, S. Puca, and W. Wagner (2016), Rainfall-runoff modelling by using SM2RAIN-derived and state-of-the-art satellite rainfall products over Italy, *Int. J. Appl. Earth Obs. Geoinf.*, *48*, 163–173.

Contractor, S., L. V. Alexander, M. G. Donat, and N. Herold (2015), How well do gridded datasets of observed daily precipitation compare over Australia? *Adv. Meteorol.*, *2015*, 325718.

Crow, W. T., G. F. Huffman, R. Bindlish, and T. J. Jackson (2009), Improving satellite rainfall accumulation estimates using spaceborne soil moisture retrievals, *J. Hydrometeorol.*, *10*, 199–212.

Crow, W. T., M. J. van den Berg, G. J. Huffman, and T. Pellarin (2011), Correcting rainfall using satellite-based surface soil moisture retrievals: The Soil Moisture Analysis Rainfall Tool (SMART), *Water Resour. Res.*, *47*, W08521, doi:10.1029/2011WR010576.

Delrieu, G., et al. (2009), Weather radar and hydrology, *Adv. Water Resour.*, *32*(7), 969–974.

Doucet, A., S. Godsill, and C. Andrieu (2000), On sequential Monte Carlo sampling methods for Bayesian filtering, *Stat. Comput.*, *10*, 197–208.

Ebert, E. E., J. E. Janowiak, and C. Kidd (2007), Comparison of near-real-time precipitation estimates from satellite observations and numerical models, *Bull. Am. Meteorol. Soc.*, *88*(1), 47–64.

FAO/IIASA/ISRIC/ISSCAS/JRC (2012), *Harmonized World Soil Database (Version 1.2)*, Food Agric. Organ., Rome and IIASA, Laxenburg, Austria. [Available at http://webarchive.iiasa.ac.at/Research/LUC/External-World-soil-database/HTML/.]

Guzzetti, F., S. Peruccacci, M. Rossi, and C. P. Stark (2007), Rainfall thresholds for the initiation of landslides in central and southern Europe, *Meteorol. Atmos. Phys.*, *98*(3–4), 239–267.

Herold, N., L. V. Alexander, M. G. Donat, S. Contractor, and A. Becker (2015), How much does it rain over land?, *Geophys. Res. Lett.*, *43*, 341–348, doi:10.1002/2015GL066615.

Hossain, F., and E. N. Anagnostou (2004), Assessment of current passive-microwave and infrared-based satellite rainfall remote sensing for flood prediction, *J. Geophys. Res.*, *109*, D07102, doi:10.1029/2003JD003986.

Hou, A. Y., R. K. Kakar, S. Neeck, A. A. Azarbarzin, C. D. Kummerow, M. Kojima, R. Oki, K. Nakamura, and T. Iguchi (2014), The Global Precipitation Measurement (GPM) mission, *Bull. Am. Meteorol. Soc.*, *95*(5), 701–722.

Huffman, G. J., R. F. Adler, D. T. Bolvin, G. Gu, E. J. Nelkin, K. P. Bowman, Y. Hong, E. F. Stocker, and D. B. Wolff (2007), The TRMM Multisatellite Precipitation Analysis (TMPA): Quasi-global, multiyear, combined-sensor precipitation estimates at fine scales, *J. Hydrometeorol.*, *8*(1), 38–55.

Hunter, P. R. (2003), Climate change and waterborne and vector-borne disease, *J. Appl. Microbiol.*, *94*(s1), 37–46.

Jones, D. A., W. Wang, and R. Fawcett (2009), High-quality spatial climate data-sets for Australia, *Aust. Meteorol. Oceanogr. J.*, *58*, 233–248.

Kerr, Y. H., et al. (2012), The SMOS soil moisture retrieval algorithm, *IEEE Trans. Geosci. Remote Sens.*, *50*(5), 1384–1403.

Kidd, C., and V. Levizzani (2011), Status of satellite precipitation retrievals, *Hydrol. Earth Syst. Sci.*, *15*, 1109–1116.

Koster, R. D., S. P. Mahanama, B. Livneh, D. P. Lettenmaier, and R. H. Reichle (2010), Skill in streamflow forecasts derived from large-scale estimates of soil moisture and snow, *Nat. Geosci.*, *3*(9), 613–616.

Krajewski, W. F., and J. A. Smith (2002), Radar hydrology: Rainfall estimation, *Adv. Water Resour.*, *25*(8), 1387–1394.

Kucera, P. A., E. E. Ebert, F. J. Turk, V. Levizzani, D. Kirschbaum, F. J. Tapiador, A. Loew, and M. Borsche (2013), Precipitation from space: Advancing Earth system science, *Bull. Am. Meteorol. Soc.*, *94*, 365–375.

Lanza, L. G., and E. Vuerich (2009), The WMO field intercomparison of rain intensity gauges, *Atmos. Res.*, *94*, 534–543.

Louvet, S., et al. (2015), SMOS soil moisture product evaluation over West-Africa from local to regional scale, *Remote Sens. Environ.*, *156*, 383–394.

Maggioni, V., P. C. Meyers, and M. D. Robinson (2016), A review of merged high resolution satellite precipitation product accuracy during the Tropical Rainfall Measuring Mission (TRMM) Era, *J. Hydrometeorol.*, *17*(4), 1101–1117.

Massari, C., L. Brocca, S. Barbetta, C. Papathanasiou, M. Mimikou, and T. Moramarco (2014), Using globally available soil moisture indicators for flood modelling in Mediterranean catchments, *Hydrol. Earth Syst. Sci.*, *18*, 839–853.

McBride, J. L., and E. E. Ebert (2000), Verification of quantitative precipitation forecasts from operational numerical weather prediction models over Australia, *Weather Forecast.*, *15*(1), 103–121.

Moradkhani, H., K.-L. Hsu, H. Gupta, and S. Sorooshian (2005), Uncertainty assessment of hydrologic model states and parameters: Sequential data assimilation using the particle filter, *Water Resour. Res.*, *41*, W05012, doi:10.1029/2004WR003604.

New, M., M. Todd, M. Hulme, and P. Jones (2001), Precipitation measurements and trends in the twentieth century, *Int. J. Climatol.*, *21*, 1899–1922.

Pellarin, T., A. Ali, F. Chopin, I. Jobard, and J.-C. Bergès (2008), Using spaceborne surface soil moisture to constrain satellite precipitation estimates over West Africa, *Geophys. Res. Lett.*, *35*, L02813, doi:10.1029/2007GL032243.

Pellarin, T., S. Louvet, C. Gruhier, G. Quantin, and C. Legout (2013), A simple and effective method for correcting soil moisture and precipitation estimates using AMSR-E measurements, *Remote Sens. Environ.*, *136*, 28–36.

Pipunic, R. C., D. Ryu, J. F. Costelloe, and C. H. Su (2015), An evaluation and regional error modeling methodology for near-real-time satellite rainfall data over Australia, *J. Geophys. Res. Atmos.*, *120*, 10,767–10,783, doi:10.1002/2015JD023512.

Rinaldo, A., E. Bertuzzo, L. Mari, L. Righetto, M. Blokesch, M. Gatto, R. Casagrandi, M. Murray, S. M. Vesenbeckh, and I. Rodriguez-Iturbe (2012), Reassessment of the 2010–2011 Haiti cholera outbreak and rainfall-driven multiseason projections, *Proc. Natl. Acad. Sci. U.S.A.*, *109*(17), 6602–6607.

Rodriguez-Fernandez, N. J., F. Aires, P. Richaume, Y. H. Kerr, C. Prigent, J. Kolassa, F. Cabot, C. Jimenez, A. Mahmoodi, and M. Drusch (2015), Soil moisture retrieval using neural networks: Application to SMOS, *IEEE Trans. Geosci. Remote Sens.*, *53*(11), 5991–6007.

Sahoo, A. K., J. Sheffield, M. Pan, and E. F. Wood (2015), Evaluation of the Tropical Rainfall Measuring Mission Multi-Satellite Precipitation Analysis (TMPA) for assessment of large-scale meteorological drought, *Remote Sens. Environ.*, *159*, 181–193.

Schamm, K., M. Ziese, A. Becker, P. Finger, A. Meyer-Christoffer, U. Schneider, M. Schröder, and P. Stender (2013), Global gridded precipitation over land: A description of the new GPCC First Guess Daily product, *Earth Syst. Sci. Data*, *6*(1), 49–60.

Scholthof, K. B. G. (2006), The disease triangle: Pathogens, the environment and society, *Nat. Rev. Microbiol.*, *5*(2), 152–156.

Serrat-Capdevila, A., J. B. Valdes, and Z. S. Eugene (2014), Water management applications for satellite precipitation products: Synthesis and recommendations, *J. Am. Water Resour. Assoc.*, *50*(2), 509–525.

Su, C.-H., D. Ryu, R. I. Young, A. W. Western, and W. Wagner (2013), Inter-comparison of microwave satellite soil moisture retrievals over Murrumbidgee Basin, southeast Australia, *Remote Sens. Environ.*, *134*, 1–11.

Tapiador, F. J., et al. (2012), Global precipitation measurement: Methods, datasets and applications, *Atmos. Res.*, *104–105*, 70–97.

Trenberth, K. E. (2014), Challenges for observing and modeling the global water cycle, *Remote Sens. Terr. Water Cycle*, *32*, 511–519.

van Dijk, A. I., H. E. Beck, R. S. Crosbie, R. A. Jeu, Y. Y. Liu, G. M. Podger, B. Timbal, and N. R. Viney (2013), The Millennium Drought in southeast Australia (2001–2009): Natural and human causes and implications for water resources, ecosystems, economy, and society, *Water Resour. Res.*, *49*, 1040–1057, doi:10.1002/wrcr.20123.

Van Leeuwen, P. J. (2009), Particle filtering in geophysical systems, *Mon. Weather Rev.*, *137*(12), 4089–4114.

Wagner, W., G. Lemoine, and H. Rott (1999), A method for estimating soil moisture from ERS scatterometer and soil data, *Remote Sens. Environ.*, *70*(2), 191–207.

Wake, B. (2013), Flooding costs, *Nat. Clim. Change*, *3*, 778.

Wanders, N., M. Pan, and E. F. Wood (2015), Correction of real-time satellite precipitation with multi-sensor satellite observations of land surface variables, *Remote Sens. Environ.*, *160*, 206–221.

Wigneron, J. P., et al. (2007), L-band Microwave Emission of the Biospehere (L-MEB) Model: Description and calibration against experimental data sets over crop fields, *Remote Sens. Environ.*, *107*(4), 639–655.

Wu, H., R. F. Adler, Y. Tian, G. J. Huffman, H. Li, and J. Wang (2014), Real-time global flood estimation using satellite-based precipitation and a coupled land surface and routing model, *Water Resour. Res.*, *50*, 2693–2717, doi:10.1002/2013WR014710.

Zhan, W., M. Pan, N. Wanders, and E. F. Wood (2015), Correction of real-time satellite precipitation with satellite soil moisture observations, *Hydrol. Earth Syst. Sci.*, *19*(10), 4275–4291.